

Underwater acoustic absorption of composite anechoic layers with inner holes

Changzheng Ye¹

State Key Laboratory for Strength and Vibration of Mechanical Structures,

Xi'an Jiaotong University, Xi'an 710049, P.R. China

MOE Key Laboratory for Multifunctional Materials and Structures,

Xi'an Jiaotong University, Xi'an 710049, P.R. China

e-mail: wdrdxz@stu.xjtu.edu.cn

Xuewei Liu¹

State Key Laboratory for Strength and Vibration of Mechanical Structures,

Xi'an Jiaotong University, Xi'an 710049, P.R. China

MOE Key Laboratory for Multifunctional Materials and Structures,

Xi'an Jiaotong University, Xi'an 710049, P.R. China

e-mail: 389626545@qq.com

Fengxian Xin²

State Key Laboratory for Strength and Vibration of Mechanical Structures,

Xi'an Jiaotong University, Xi'an 710049, P.R. China

MOE Key Laboratory for Multifunctional Materials and Structures,

Xi'an Jiaotong University, Xi'an 710049, P.R. China

Corresponding author e-mail: fengxian.xin@gmail.com or fxxin@mail.xjtu.edu.cn

Tian Jian Lu

State Key Laboratory of Mechanics and Control of Mechanical Structures,

Nanjing University of Aeronautics and Astronautics, Nanjing 210016, P.R. China

State Key Laboratory for Strength and Vibration of Mechanical Structures,

Xi'an Jiaotong University, Xi'an 710049, P.R. China

e-mail: tjlu@nuaa.edu.cn

Abstract: A combined theoretical and numerical study is carried out to quantify the influence of material properties (e.g. real part and loss factor of Young's modulus, material density) and geometrical parameters (e.g., layer thickness, height of hole) on

¹The authors contributed equally to this work.

²Corresponding author.

the sound absorption performance of an underwater rubber layer containing periodically distributed axial holes. A theoretical model is developed based on the method of transfer matrix as well as the concept of equivalent layering of holes with variable cross-section. Numerical simulations with the method of finite elements are subsequently carried out to validate the theoretical model, with good agreement achieved. Physical mechanisms underlying the enhanced acoustic performance of the anechoic layer as a result of introducing the periodic holes are explored in terms of the generated transverse waves and the high order mode of vibration. The results presented are helpful for designing high-performance underwater acoustic layers with periodically distributed cavities by tailoring relevant material properties and geometrical parameters.

Keywords: Composite anechoic layer; Periodic holes; Sound absorption; Analytical modeling; Finite element simulation

1. Introduction

The acoustic absorption property is an important functionality of various composite materials/structures, which can be tailored via the reasonable design of their micro-structure and macro-geometry [1-4]. As a typical composite material or structure, the underwater anechoic layer is usually made up of a rubber matrix containing periodically distributed holes, which possesses excellent acoustic absorption performance in underwater environments. Early research on underwater sound attenuation dated from the theoretical study of oscillations and wave propagation in solid media with inner holes [5-7]. Thereafter, two types of resonance mechanism were identified [8,9] for Alberich anechoic layer, which is a viscoelastic medium containing short cylindrical holes. One is the radial motion of the hole wall and the other is the drum-like oscillations of the cover layer.

Modern anechoic layers typically have the structure of multilayers, or can be equivalent to multilayered coatings. Consequently, theoretical modeling of such anechoic layers usually calls for the transfer matrix method to establish the acoustic relationship between the two sides of the layer. For typical instance, Cervenka *et al.* [10] deduced the transfer matrix of a multilayered structure where each layer can be either liquid or solid, so that the acoustic performance of the structure could be efficiently evaluated [11]. Nowadays, gradually varied axial holes such as

conical and horn holes are often adopted to enhance the sound absorption performance of underwater anechoic layers. Built upon the model of wave propagation in cylindrical tube [12] as well as the equivalent model of layering for gradually varied axial holes [13], the sound properties of such anechoic layers can be theoretically characterized using the transfer matrix method. Moreover, the underwater acoustic performance of the anechoic layers attached with rib-stiffened plate was theoretically investigated by the well-developed elasticity models [14-16], which considered the effect of the periodical rib-stiffeners. Besides the above mentioned theoretical analyses, the numerical method of finite elements (FE) has also been developed to calculate the acoustic performance of anechoic layers. For instance, based on FE simulations, Hennion *et al.* [17] and Easwaran *et al.* [18] investigated the scattering and reflection characteristics of anechoic layers containing doubly periodic holes, while Panigrahi *et al.* [19] compared anechoic coatings with different sizes of air channels (holes) adhered on the same side or different sides of a steel plate.

Although there exist numerous theoretical and numerical researches on the underwater sound absorption of composite anechoic layers, comprehensive studies on the influence of material properties and geometrical parameters on the acoustic performance of an composite anechoic layer containing gradually varied axial holes are scarce. Further, the absorption mechanism for waterborne sound in composite anechoic layers containing periodically distributed holes needs to be further explored, which is of vital importance for the design of the microstructure of the composite anechoic layers toward to superior underwater acoustic absorption. This paper aims to address these issues using a combined approach of theoretical analysis and numerical (FE) calculation.

2. Theoretical model

Figure 1(a) displays the cross-sectional configuration and working condition of a representative underwater anechoic layer containing periodically distributed holes, which is adhered to a steel plate. The lateral size of the whole structure including the anechoic layer and the steel plate is assumed to be infinite. The mediums at the two sides of the anechoic layer-steel plate structure are air and water, respectively, both considered to be spatially semi-infinite. When a normally incident plane sound wave propagates from the far field in the water into the anechoic layer, the wave is attenuated. As the steel plate is supposed to be a rigid back, the wave completely reflects back, eventually into the water.

For simplicity, regular triangular arrangement of the holes in the anechoic layer is adopted, as shown in Fig. 1(b). Due to periodical distribution of the holes, only a single cell with hexagonal perimeter needs to be extracted for further study. However, the hexagonal unit cell is difficult to be analyzed theoretically. To overcome the difficulty, a simplification method is introduced in Fig. 1(c). With no deformation of the hole, the external morphology of the unit cell is assumed to transform from the original hexagonal shape to a cylindrical one, with the volume unchanged. As a result, the gradually varying axial hole may be taken as equivalent to a cluster of shallow cylindrical holes for which analytical solution can be obtained. The analytical solution will be accurate enough so long as the segments of Fig. 1(c) are divided densely enough. Figure 2 depicts one such segment, i.e., a cylindrical pipe. Due to axial symmetry, the cylindrical coordinate system rOz is adopted. The inner and outer radii of the pipe are denoted as a and b and the length as l .

The anechoic layer is made up of rubber, which is a linear viscoelastic material. For the case of harmonic incident wave, the vibrating governing equation can be written in the same form as that of an elastic material [20]:

$$\mu u_{i,jj} + (\lambda + \mu) u_{j,ji} = \rho \ddot{u}_i \quad (1)$$

where u is the displacement, λ and μ are the Lamé constants, and ρ is the density of rubber. As usual, the summation convention is implied. For rubber, λ and μ are complex numbers while ρ is a real number.

The displacement vector \mathbf{u} can be written in a decomposition form, as [20]:

$$\mathbf{u} = \nabla \zeta + \nabla \times \boldsymbol{\xi} \quad (2)$$

where ζ is a scalar potential function and $\boldsymbol{\xi}$ is a vector potential function. The former is related to longitudinal wave while the latter is related to transverse wave. In consideration of the axial symmetry, there is no circumferential component of the transverse wave and so does the second term of \mathbf{u} . Thus, the vector potential function $\boldsymbol{\xi}$ can be degenerated to a scalar potential function ξ .

Equations (2) is satisfied by the Helmholtz equations,

$$\begin{aligned} (\nabla^2 + K_1^2) \zeta &= 0 \\ (\nabla^2 + K_2^2) \xi &= 0 \end{aligned} \quad (3)$$

where K_1 and K_2 are the longitudinal wavenumber and the transverse wavenumber, respectively.

The solution of equations (3) can be written as (time-depending term omitted for brevity):

$$\begin{aligned}\zeta &= [C_1 J_0(k_1 r) + C_2 Y_0(k_1 r)] e^{ikz} \\ \xi &= [C_3 J_0(k_2 r) + C_4 Y_0(k_2 r)] e^{ikz}\end{aligned}\quad (4)$$

where C_1 to C_4 are four undetermined coefficients; k is the axial wavenumber; $k_1 = \sqrt{K_1^2 - k^2}$ and $k_2 = \sqrt{K_2^2 - k^2}$ are the radial wavenumbers of longitudinal wave and transverse wave, respectively; and $J_0(\)$ and $Y_0(\)$ are the Bessel functions of the first kind and the second kind, respectively.

In the cylindrical coordinate system, the radial component of displacement, u_r , and the axial component of displacement, u_z , have the following expressions:

$$\begin{aligned}u_r &= \frac{\partial \zeta}{\partial r} + \frac{\partial^2 \xi}{\partial r \partial z} \\ u_z &= \frac{\partial \zeta}{\partial z} - \frac{\partial^2 \xi}{\partial r^2} - \frac{\partial \xi}{r \partial r}\end{aligned}\quad (5)$$

According to equations (4) and (5) as well as the geometric equations and constitutive relation, the relation between the three variables, u_r , σ_r and τ_{rz} , and the four undetermined coefficients, C_1 to C_4 , can be expressed as:

$$\begin{Bmatrix} u_r \\ \sigma_r \\ \tau_{rz} \end{Bmatrix} = e^{ikz} \begin{bmatrix} M_{11} & M_{12} & M_{13} & M_{14} \\ M_{21} & M_{22} & M_{23} & M_{24} \\ M_{31} & M_{32} & M_{33} & M_{34} \end{bmatrix} \begin{Bmatrix} C_1 \\ C_2 \\ C_3 \\ C_4 \end{Bmatrix}\quad (6)$$

where σ_r is the normal stress and τ_{rz} is the shear stress. Expressions of the twelve elements in the coefficient matrix of (7) are presented in the Appendix.

Consider next the boundary conditions for the cylindrical pipe of Fig. 2 Due to periodical arrangement of holes in the anechoic layer, the interface between two adjacent cells - which is also the outer boundary of each cell - should comply with the symmetric boundary condition. Besides, since the impedance of air (i.e., medium in the hole) is far less than that of rubber (i.e., matrix material of the anechoic layer), the inner boundary of each cell can be considered as a free interface. Therefore, the boundary conditions are given by:

$$\begin{cases} \sigma_r|_{r=a} = 0, & \sigma_{rz}|_{r=a} = 0 \\ u_r|_{r=b} = 0, & \sigma_{rz}|_{r=b} = 0 \end{cases} \quad (8)$$

Upon substituting (8) into (6), the equations for C_1 to C_4 are obtained, as:

$$\begin{bmatrix} M_{11}(b) & M_{12}(b) & M_{13}(b) & M_{14}(b) \\ M_{21}(a) & M_{22}(a) & M_{23}(a) & M_{24}(a) \\ M_{31}(a) & M_{32}(a) & M_{33}(a) & M_{34}(a) \\ M_{31}(b) & M_{32}(b) & M_{33}(b) & M_{34}(b) \end{bmatrix} \begin{Bmatrix} C_1 \\ C_2 \\ C_3 \\ C_4 \end{Bmatrix} = \mathbf{0} \quad (9)$$

where a and b in the parentheses represent the value of r in each element.

For equation (9) to have a non-zero solution, the determinant of its coefficient matrix must equal to zero. The axial wavenumbers can thence be solved; while only the lowest order wavenumber k are considered here, because it has the most significant influence on the sound absorption performance of the cylindrical pipe (Fig. 2) in low frequencies [13]. In this way, the transfer matrix shown in Eq. (10) then can be used. If the considered frequency is too high, higher order wavenumbers need to be considered, but the transfer matrix will be not feasible.

To proceed further, each segment containing a cylindrical hole (Fig. 2) is taken as equivalent to a homogeneous material with corresponding effective parameters. For the i th segment, its effective wavenumber is equal to the axial wavenumber, notated as k_i , while its effective density is the volumetric average value, notated as ρ_i . Once this is done, the transfer matrix method can be adopted to establish the relation between the two sides of the anechoic layer that contains say a total of n such segments.

Let the interface between the anechoic layer and the water medium denote the front interface of the anechoic layer, and let the interface between the anechoic layer and the steel plate denote the back interface. The transfer matrix of the i th segment has thence the following expression,

$$\mathbf{T}_i = \begin{bmatrix} \cos(k_i l_i) & -\frac{i\omega\rho_i}{k_i} \sin(k_i l_i) \\ -\frac{ik_i}{\omega\rho_i} \sin(k_i l_i) & \cos(k_i l_i) \end{bmatrix} \quad (10)$$

where l_i is the thickness of the i th segment. The total transfer matrix of the anechoic layer becomes therefore:

$$\mathbf{T} = \begin{bmatrix} T_{11} & T_{12} \\ T_{21} & T_{22} \end{bmatrix} = \prod_{i=1}^n \mathbf{T}_i \quad (11)$$

In accordance with the transfer matrix method, the acoustic pressure and vibration velocity at the front interface, p_f and v_f , and those at the back interface, p_b and v_b , can be related by \mathbf{T} , as:

$$\begin{Bmatrix} p_f \\ v_f \end{Bmatrix} = \mathbf{T} \begin{Bmatrix} p_b \\ v_b \end{Bmatrix} = \begin{bmatrix} T_{11} & T_{12} \\ T_{21} & T_{22} \end{bmatrix} \begin{Bmatrix} p_b \\ v_b \end{Bmatrix} \quad (12)$$

Since the steel plate is considered rigid, the impedance of the back interface $Z_b = p_b/v_b = \infty$. Thus, according to (12),

$$Z_f = \frac{p_f}{v_f} = \frac{T_{11}}{T_{21}} \quad (13)$$

Finally, due to the relation between the reflection coefficient and the acoustic impedance, as well as energy conservation, the sound absorption coefficient α of the anechoic layer is obtained as:

$$\alpha = 1 - \left| \frac{Z_f - \rho_w c_w}{Z_f + \rho_w c_w} \right|^2 \quad (14)$$

where ρ_w and c_w are the density and sound speed of water, respectively.

3. Results and discussion: parameter studies

3.1 Geometric and material parameters of anechoic layer

To characterize the acoustic performance of the anechoic layer and explore the underlying sound absorption mechanisms based on the theoretical model developed in the previous section, the parameters that are varied include: rubber density, real part of Young's modulus, loss factor of Young's modulus, thickness of anechoic layer, and height of bore hole. To this end, two different types of hole – cylindrical bore and conical bore – are considered, as illustrated in Fig. 3, with fixed geometrical parameters as: radius of unit cell $r_a = 15$ mm; $p_{\text{cylinder}} = 4$ mm; $p_{\text{cone}} = 3$ mm; $q_{\text{cone}} = 7$ mm.

Table 1 lists relevant material and geometric parameters of anechoic layers considered in the present study, in which the parameters with only one value are the fixed ones while those with three values will be varied in the calculations presented below. Values with an asterisk are the

default ones, which means that when one parameter is discussed (varied), the remaining parameters take default values.

3.2 Effect of rubber density

The effect of rubber density on sound absorption is quantified in Fig. 4 for both cylindrical and conical holes. Their corresponding homogenous layers containing no holes are also plotted for demonstrating the effective frequency range of perforating holes in rubber. In addition to sound absorption curves calculated using the present theoretical model, the curves calculated directly by FEM (finite element method) with COMSOL are included for comparison. In the numerical simulations, the rubber domain is simulated by the "Elastic waves" physical field in COMSOL while the air domain in the hole as well as the external water domain are simulated by the "Pressure acoustics" physical field in COMSOL. The "Acoustic-structure boundary" is set between the fluid and rubber to ensure the continuity of the particle acceleration and sound pressure in the normal direction of the boundary, as below:

$$-\mathbf{n} \cdot \left(-\frac{1}{\rho_c} (\nabla p_t - \mathbf{q}_d) \right) = -\mathbf{n} \cdot \mathbf{u}_t \quad (15)$$

$$\mathbf{F}_A = p_t \mathbf{n}$$

where \mathbf{u}_t is the particle acceleration, \mathbf{n} is the unit vector of surface normal, p_t is the total sound pressure, \mathbf{F}_A is the load (force per unit area) experienced by the structure, \mathbf{q}_d is the dipole source.

Here, the considered frequency range is considered below 10kHz, because the low frequency sound absorption performance of the anechoic layers is of great concern for underwater sound propagation. The results of Fig. 4 (as well as those presented in Figs.5 to 8) demonstrate that excellent agreement between theoretical prediction and FEM simulation is achieved before 5 kHz, while small deviations exist at higher frequencies because only the lowest order axial wavenumber is considered for each divided cylindrical pipe as mentioned above. Although these deviations slowly become larger at higher frequencies, the theoretical results can also give good predictions and right curve tendencies.

As shown in Fig. 4, two absorption peaks exist within the studied frequency range for both the cylindrical hole case and conical hole case. These two cases also have similar curve tendencies. For the default cylindrical hole case, the first absorption peak is at 2 kHz with a relatively lower peak coefficient reaching 0.42; while the second peak is at about 8.9 kHz with a relatively higher peak coefficient nearly reaching 1. For the default conical hole case, its two

peaks (the first at 1.4 kHz and the second at 8.5 kHz) are both earlier than those of the default cylindrical hole case. This is because the conical case has a larger hole volume, which means its structural stiffness is smaller, leading to lower resonance absorption peaks, especially for the first peak in a relatively lower frequency range, i.e. the stiffness region where the absorption performance is mainly influenced by the stiffness.

In Fig. 4, comparing the anechoic layers containing holes with the corresponding homogenous layers, it is found that the homogenous layer has a relatively smooth absorption curve like a homogenous porous material for air-borne sound absorption, the perforating holes in homogenous rubber layers improves the absorption performance at relatively low and high frequency region in the studied frequency range. For the default cylindrical case, its absorption performance is enhanced within 0-3 kHz and 7-10 kHz. Although an absorption decline occurs in middle frequency range, the average absorption coefficient in the whole studied frequency range is obviously improved. This phenomenon is in some degree like perforating holes in high resistivity homogenous porous materials to form double porosity materials [21], which are both contributed to the improvement of the acoustic impedance matching between the absorbing material and the surrounding media.

As to the effects of rubber density on the absorption performance of anechoic layers, when rubber density is varied, the absorption curves of Fig. 4(a) for cylindrical holes exhibit similar variation trend as those of Fig. 4 (b) for conical holes. Take Fig. 4(a) for example. When rubber density is increased, the absorption coefficient remains almost unchanged from 0 to about 1 kHz, increases slightly from about 1 to 5 kHz, and obviously increases from about 5 to 8 kHz. As mentioned above, the low-frequency (stiffness region) absorption performance is mainly influenced by the structural stiffness, and barely influenced by mass, i.e. density. With the frequency increasing, density's influences grow, and a larger mass brings the vibration mode (i.e. the second peak here) towards lower frequencies. Thus, within the frequency range considered in the present study, rubber density has significant influence on sound absorption only at middle and high frequencies.

3.3 Effect of the real part of rubber Young's modulus

Figure 5 displays the effect of the real part of the rubber Young's modulus on the acoustic performance of the anechoic layer. Different with the effect of rubber density, the real part of the Young's modulus influences the absorption curve from the initial frequencies. As the real part of

Young's modulus is increased, the absorption coefficient slightly decreases before about 1.5 kHz. Then, from about 2 to 5 kHz, enhanced absorption is observed; while, beyond about 6 kHz, the absorption is significantly deteriorated. At high frequencies, the crests of the curves are almost at the same level. In general, as the real part of Young's modulus is increased, the stiffness of anechoic layers increases and induces the vibration modes' absorption peaks as well as the whole absorption curve moving to higher frequencies. As shown in Fig. 5, for the three cylindrical cases, as the real part of the Young's modulus increases, the first peak frequency ranges from about 1.5 to 2.5 kHz, and the second peak frequency ranges from about 8 to 10 kHz; for the three conical cases, the first peak frequency ranges from about 1 to 1.8 kHz, and the second peak frequency ranges from about 7.5 to 9.5 kHz. Moreover, it is worth noting that although decreasing the real part of the rubber Young's modulus can bring the whole absorption curve towards lower frequencies, the first absorption peak and first absorption valley both become lower. In addition, for the homogenous rubber layers containing no holes, a smaller Young's modulus case has a better absorption performance at lower frequencies (0-5 kHz here) but a worse performance at higher frequencies (5-10 kHz here).

3.4 Effect of the loss factor of rubber Young's modulus

Besides the real part, the Young's modulus of a viscoelastic material has another component, the loss factor. The effect of the loss factor on sound absorption is presented in Fig. 6 for both hole types. It is apparent that, as the loss factor is increased (from 0.17 to 0.29), the absorption curve has a prominent broadband enhancement between 0.5 kHz to about 6.5 kHz; although the first peak frequency is almost unchanged, the peak coefficient increases from about 0.33 to 0.5 for both the cylindrical cases and conical cases. At higher frequencies (> 7 kHz), however, the loss factor has considerably diminished influence.

The loss factor is the ratio of the imaginary part of rubber Young's modulus to its real part. The real part is also known as the storage modulus of rubber, while the imaginary part represents the loss modulus of rubber. Because in this section the loss factor is the only variable, which means the real part is fixed, the imaginary part increases as the loss factor is increased. Increasing the loss factor will therefore directly increase the energy dissipation capacity of the rubber material itself. That is, the mechanical energy of sound wave's vibration is increasingly converted into heat via viscoelastic dissipation, increasing thus the absorption coefficient. This is also the reason of absorption enhancement for homogenous layers containing no holes. Moreover, as

shown in Fig. 6, the loss factor has the largest influence on anechoic layers' sound absorption at the peak frequency, which is consistent with the common sense: damping has the largest influence around the resonance frequency where is often called damping region. While for the second peak, as the absorption coefficient has almost reached 1, the damping's effect is not obvious.

3.5 Effect of rubber layer thickness

Apart from material parameters, geometric parameters also play a significant role in the acoustic performance of an anechoic layer. In this section, the effect of rubber layer thickness is both theoretically predicted and numerically calculated, as shown in Fig. 7. As the thickness is increased from 50 mm to 90 mm, the absorption curve rises at all the frequencies, especially in two particular bands. The first band ranges from about 1 to 2 kHz, covering the first crest of the curve. The second band ranges from about 4 to 8 kHz, during which the absorption coefficient rises from the trough to the second crest of the curve. The enhancement in sound absorption at all the frequencies is easily understandable, because the amount of rubber material available for sound energy absorption increases when the anechoic layer is thickened.

3.6 Effect of hole height

With the thickness of anechoic layer fixed, the influence of hole height on sound absorption is shown in Fig. 8 for both cylindrical and conical holes. As the hole height is increased from 20 mm to 40 mm, the absorption peaks move to low frequencies, but meanwhile with a lower first peak and valley. The absorption coefficient increases mildly at frequencies less than about 1.5 kHz, decreases in the frequency band from about 2 to 5.5 kHz, and exhibits a huge growth after about 8 kHz.

It is seen from Fig. 8 that the effect of hole height is most distinct at high frequencies. Further, increasing the hole height shifts the absorption curve towards lower frequencies, which is contrary to that caused by increasing the real part of Young's modulus, but the reason might be similar: as the hole height is increased, the total stiffness of the anechoic layer decreases, so that the curve as a whole tends to move towards the direction of low frequencies.

4. Absorption mechanisms of underwater anechoic layer with inner holes

To reveal the physical mechanisms underlying sound absorption, the numerically simulated displacement contours in the rubber domain containing periodic cylindrical holes are presented below for selected frequencies. For normal incident sound, the longitudinal wave and the transverse wave are independent along the axial direction and the radial direction, respectively. In

contrast, in the case of conical and horn holes, the longitudinal and transverse waves are coupled with each other along the axial and radial directions. Thus, cylindrical holes can better reveal the influence of longitudinal and transverse waves upon sound absorption.

For convenience, unit stimulation is adopted in the simulation, which means that the initial incidence sound pressure is 1 Pa. Fig. 9 and Fig. 10 display the displacement contours in rubber domain with different thicknesses of anechoic layer and different hole heights, respectively. Note that the sound incidence wave propagates from the bottom (water domain) of each cell and the upper surface of each cell is fixed to the steel plate. It can be seen from these displacement contours that radial displacement in rubber only exists in the region containing the cylindrical hole: that is, there is no radial displacement in the rubber domain without any hole. Since the radial displacement stands for the vibration amplitude of the transverse wave, the present results testify that it is the existence of the hole that generates the transverse wave. Moreover, in viscoelastic materials like rubber, the energy dissipation capacity of the transverse wave is stronger than that of the longitudinal wave. Therefore, the presence of holes, be it cylindrical or conical, leads to enhanced dissipation of acoustic energy in the rubber layer.

At low frequencies, the vibration of rubber in each cell is in the low order mode. From Fig. 9(a) and Fig. 10(a), the axial displacement are seen to vary almost exclusively along the axial direction, and at the same time, the radial displacement varies almost exclusively along the radial direction. Whereas, at high frequencies, the vibration in each cell is in the high order mode. As shown in Fig. 9(b) and Fig. 10(b), the axial and radial displacement vary not only along the axial direction but also along the radial direction. However, the axial displacement contours of Fig.9(b) and Fig. 10(b) demonstrate that the axial high order mode only exists in the region containing the cylindrical hole. In the region without the presence of any hole, the vibration is still in the low order mode, although it occurs at high frequencies. Hence, it is the presence of holes that generates the high order mode of vibration, enhancing further the dissipation of acoustic energy.

Furthermore, the energy dissipation is strongly related with the rubber deformation gradient distribution, because the larger deformation gradient means larger friction energy dissipation. From this point of view, the sound absorption performance of these anechoic layers can be evaluated by the displacement distributions shown in Figs. 9 and 10. As seen from Fig. 9, the rubber deformation distributions near the hole for different thickness cases are similar at the same frequency, in such case, a larger volume with no holes will cause more energy dissipation,

therefore the anechoic layer of 90mm thickness always has the best sound absorption performance among the three cases, as shown in Fig. 7. As seen from Fig. 10(a), at the frequency of 4kHz, the deformation gradient has the relationship: the 20mm case larger than the 30mm case and larger than the 40mm case, which leads to the same trends of the sound absorption performance in Fig. 8(a). Also, in Fig. 10(b), at the frequency of 9kHz, the deformation gradient has the relationship: the 40mm case larger than the 30mm case and larger than the 20mm case, correspondingly, the sound absorption performance has the same trends in Fig. 8(b).

5. Conclusions

A combined theoretical and numerical study is carried out to quantify the influence of material and geometric parameters on the sound absorption performance of underwater rubber layers containing periodically distributed axial holes. Physical mechanisms underlying the enhanced performance of the anechoic layer as a result of introducing the periodic holes are also explored. The main conclusions drawn are: (1) Within the frequency range considered, increasing the density of rubber enhances sound absorption at middle and high frequencies (from 4 kHz to 10 kHz), whereas it has little difference on the sound absorption at relatively low frequencies (< 4 kHz). (2) Increasing the real part of rubber Young's modulus shifts the absorption curve as a whole towards higher frequencies. (3) Increasing the loss factor of rubber Young's modulus leads to prominent broadband absorption enhancement at relatively low and middle frequencies (between 0.5 kHz to about 6.5 kHz). (4) Increasing the thickness of rubber layer enhances sound absorption at all frequencies, especially at low frequencies and high frequencies. (5) Increasing the height of axial holes shifts the absorption curve towards lower frequencies, which is just opposite to that caused by increasing the real part of Young's modulus. (6) The presence of periodically distributed axial holes generates transverse wave as well as high order mode of vibration in the rubber layer, thus beneficial for sound energy dissipation. The results presented in this study are helpful for designing high-performance underwater acoustic layers with periodically distributed cavities by tailoring the material properties and geometrical parameters of the layer.

Appendix

Explicit expressions of the twelve elements in the coefficient matrix of Eq. (6) are:

$$M_{11} = -k_1 J_1(k_1 r) \quad (A1)$$

$$M_{12} = -k_1 Y_1(k_1 r) \quad (A2)$$

$$M_{13} = -i k k_2 J_1(k_2 r) \quad (A3)$$

$$M_{14} = -i k k_2 Y_1(k_2 r) \quad (A4)$$

$$M_{21} = -\left[\lambda(k_1^2 + k^2) + 2\mu k_1^2 \right] J_0(k_1 r) + \frac{2\mu k_1}{r} J_1(k_1 r) \quad (A5)$$

$$M_{22} = -\left[\lambda(k_1^2 + k^2) + 2\mu k_1^2 \right] Y_0(k_1 r) + \frac{2\mu k_1}{r} Y_1(k_1 r) \quad (A6)$$

$$M_{23} = 2i\mu k_2 k \left[-k_2 J_0(k_2 r) + \frac{1}{r} J_1(k_2 r) \right] \quad (A7)$$

$$M_{24} = 2i\mu k_2 k \left[-k_2 Y_0(k_2 r) + \frac{1}{r} Y_1(k_2 r) \right] \quad (A8)$$

$$M_{31} = -2i\mu k_1 k J_1(k_1 r) \quad (A9)$$

$$M_{32} = -2i\mu k_1 k Y_1(k_1 r) \quad (A10)$$

$$M_{33} = \mu k_2 (k^2 - k_2^2) J_1(k_2 r) \quad (A11)$$

$$M_{34} = \mu k_2 (k^2 - k_2^2) Y_1(k_2 r) \quad (A12)$$

Acknowledgements

This work was supported by NSFC (11761131003, U1737107 and 11772248), DFG (ZH15/32-1) and the Fundamental Research Funds for the Central Universities (Z201811253).

References

- [1] Kim, B.-S., Cho, S.-J., Min, D.-k., and Park, J., 2016, "Experimental study for improving sound absorption of a composite helical-shaped porous structure using carbon fiber," *Composite Structures*, **145**, pp. 242-247.
- [2] Ogam, E., Fella, Z. E. A., and Ogam, G., 2016, "Identification of the mechanical moduli of closed-cell porous foams using transmitted acoustic waves in air and the transfer matrix method," *Composite Structures*, **135**, pp. 205-216.
- [3] Ren, S., Ao, Q., Meng, H., Xin, F., Huang, L., Zhang, C., and Lu, T. J., 2017, "A semi-analytical model for sound propagation in sintered fiber metals," *Composites Part B-*

- Engineering, **126**, pp. 17-26.
- [4] Xin, F. X., and Lu, T. J., 2016, "Acoustomechanical constitutive theory for soft materials," *Acta Mechanica Sinica*, **32**(5), pp. 828-840.
- [5] Blake, F. G., 1952, "Spherical wave propagation in solid media," *Journal of the Acoustical Society of America*, **24**(2), pp. 211-214.
- [6] Meyer, E., Brendel, K., and Tamm, K., 1958, "Pulsation oscillations of cavities in rubber," *Journal of the Acoustical Society of America*, **30**(12), pp. 1116-1124.
- [7] White, R. M., 1957, "Radiation impedance of a cylindrical bore in a solid," *Journal of the Acoustical Society of America*, **29**(6), pp. 751-752.
- [8] Gaunard, G., 1985, "Comments on 'Absorption mechanisms for waterborne sound in Alberich anechoic layers'," *Ultrasonics*, **23**(2), pp. 90-91.
- [9] Lane, R., 1981, "Absorption mechanisms for waterborne sound in Alberich anechoic layers," *Ultrasonics*, **19**(1), pp. 28-30.
- [10] Cervenka, P., and Challande, P., 1991, "A new efficient algorithm to compute the exact reflection and transmission factors for plane waves in layered absorbing media (liquids and solids)," *Journal of the Acoustical Society of America*, **89**(4), pp. 1579-1589.
- [11] Liang, G., and Pang, F., 2013, "Acoustic characteristics of underwater composite materials at oblique incidence of sound wave," *Noise & Vibration Worldwide*, **44**(5), pp. 12-17.
- [12] Sinha, B. K., Plona, T. J., Kostek, S., and Chang, S.-K., 1992, "Axisymmetric wave propagation in fluid-loaded cylindrical shells. I: Theory," *Journal of the Acoustical Society of America*, **92**(2), pp. 1132-1143.
- [13] Tao, M., 2014, "Simplified model for predicting acoustic performance of an underwater sound absorption coating," *Journal of Vibration and Control*, **20**(3), pp. 339-354.
- [14] Xin, F., and Lu, T. J., 2017, "A plane strain elasticity model for the acoustical properties of rib-stiffened composite plates," *European Journal of Mechanics-A/Solids*, **62**, pp. 1-13.
- [15] Xin, F. X., 2015, "Signal response of rib-stiffened plates covered by decoupling coating layers," *Journal of Sound and Vibration*, **348**, pp. 206-223.
- [16] Xin, F. X., 2015, "An exact elasticity model for rib-stiffened plates covered by decoupling acoustic coating layers," *Composite Structures*, **119**, pp. 559-567.
- [17] Hladky-Hennion, A.-C., and Decarpigny, J.-N., 1991, "Analysis of the scattering of a plane acoustic wave by a doubly periodic structure using the finite element method: Application to

- Alberich anechoic coatings," *Journal of the Acoustical Society of America*, **90**(6), pp. 3356-3367.
- [18]Easwaran, V., and Munjal, M. L., 1993, "Analysis of reflection characteristics of a normal incidence plane wave on resonant sound absorbers: A finite element approach," *Journal of the Acoustical Society of America*, **93**(3), pp. 1308-1318.
- [19]Panigrahi, S. N., Jog, C. S., and Munjal, M. L., 2008, "Multi-focus design of underwater noise control linings based on finite element analysis," *Applied Acoustics*, **69**(12), pp. 1141–1153.
- [20]Achenbach, J. D., 1973, *Wave propagation in elastic solids*, North-Holland Publishing Company, Amsterdam, London.
- [21]Olny, X., and Boutin, C., 2003, "Acoustic wave propagation in double porosity media," *Journal of the Acoustical Society of America*, **114**(1), pp. 73-89.

List of figure captions

Fig. 1 (Color online) Schematic of a underwater anechoic layer: (a) cross-sectional configuration and working condition; (b) spatial distribution of holes; (c) equivalence of unit cell

Fig. 2 (Color online) Acoustic cylindrical pipe

Fig. 3 (Color online) Anechoic layer with (a) cylindrical hole and (b) conical hole

Fig. 4 (Color online) Effect of rubber density on sound absorption: (a) cylindrical hole; (b) conical hole

Fig. 5 (Color online) Effect of the real part of rubber Young's modulus on sound absorption: (a) cylindrical hole; (b) conical hole

Fig. 6 (Color online) Effect of the loss factor of Young's modulus on sound absorption: (a) cylindrical hole; (b) conical hole

Fig. 7 (Color online) Effect of anechoic layer thickness on sound absorption: (a) cylindrical hole; (b) conical hole

Fig. 8 (Color online) Effect of hole height on sound absorption: (a) cylindrical hole; (b) conical hole

Fig. 9 (Color online) Displacement contours in rubber layer with different thicknesses at: (a) 1.5 kHz (unit: 10^{-11} m); (b) 6 kHz (unit: 10^{-12} m)

Fig. 10 (Color online) Displacement contours in rubber layer with different hole heights at: (a) 4 kHz (unit: 10^{-11} m); (b) 9 kHz (unit: 10^{-11} m)

List of tables

Table 1 Material and geometric parameters

Accepted Manuscript Not Copyedited

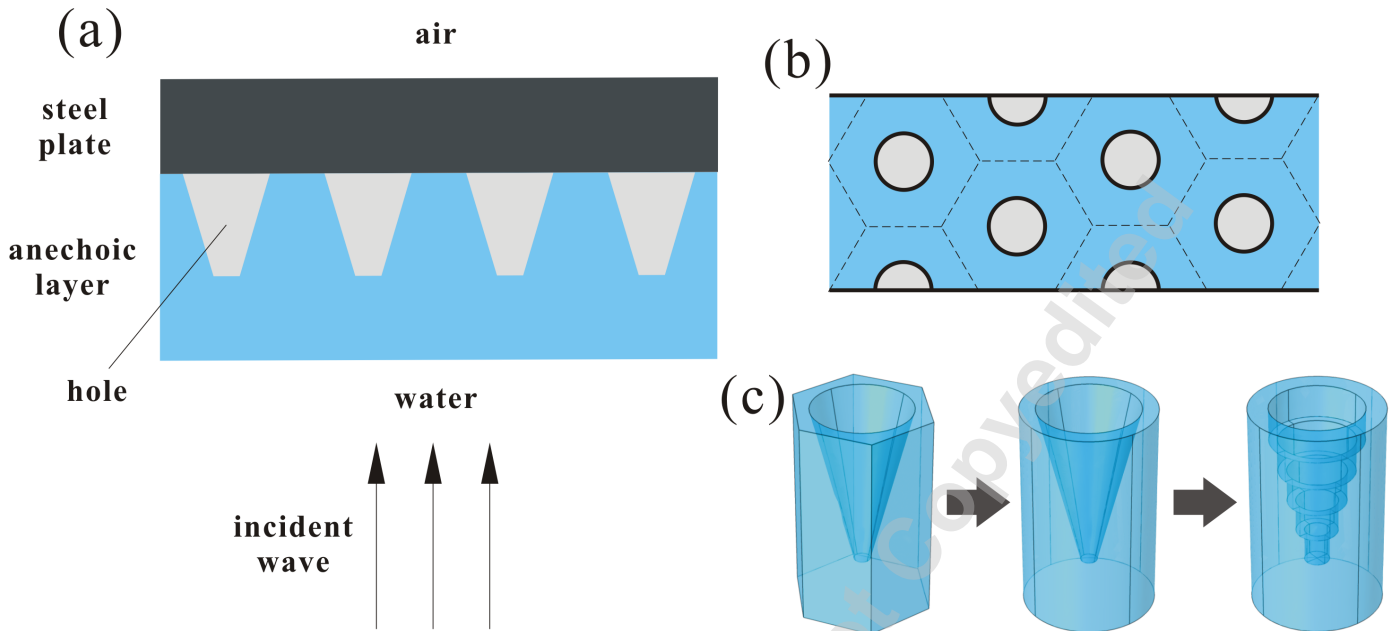


Fig. 1

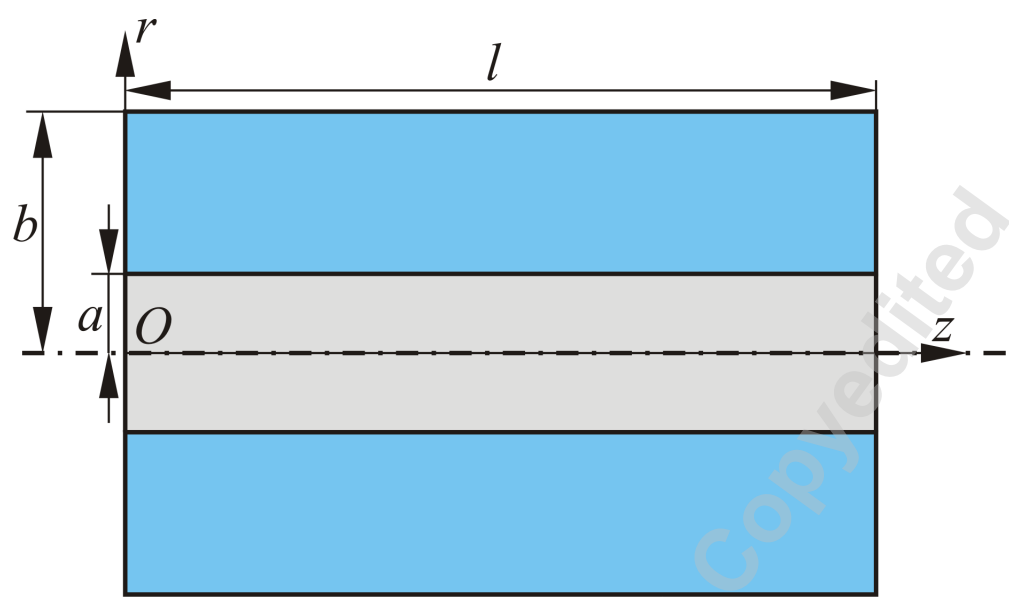


Fig. 2

Accepted Manuscript Not Copyedited

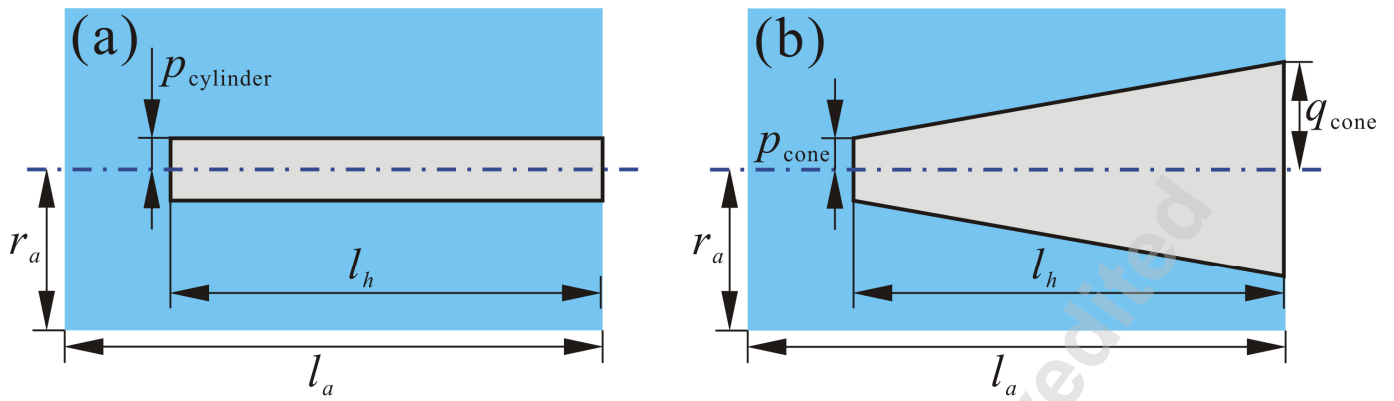


Fig. 3

Accepted Manuscript Not Copyedited

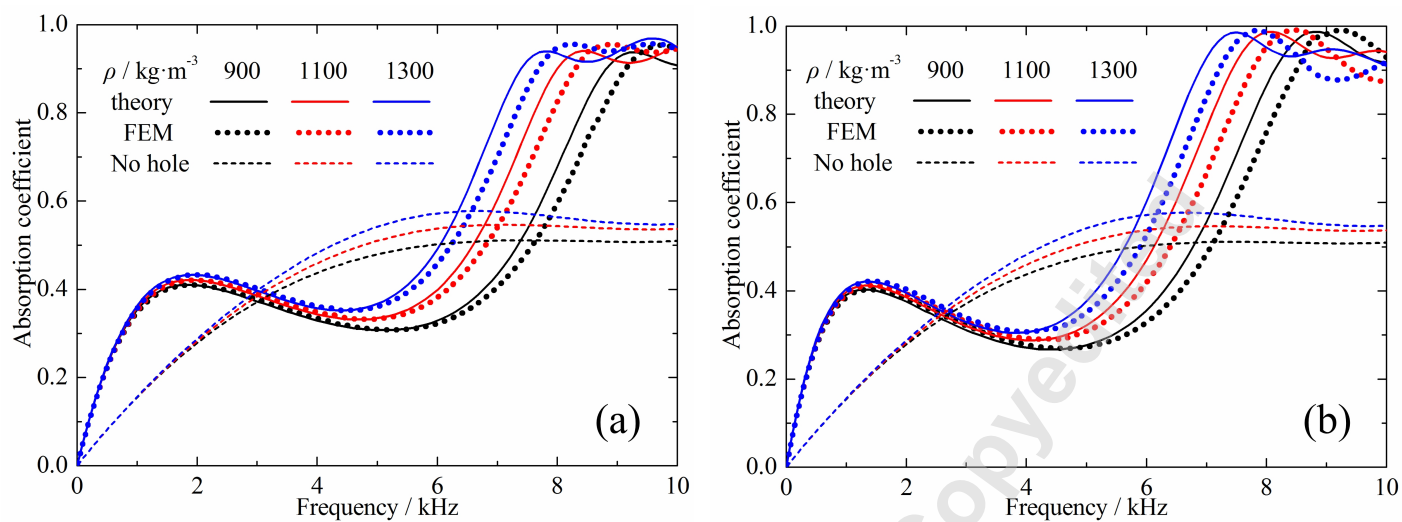


Fig. 4

Accepted Manuscript Not Copyable

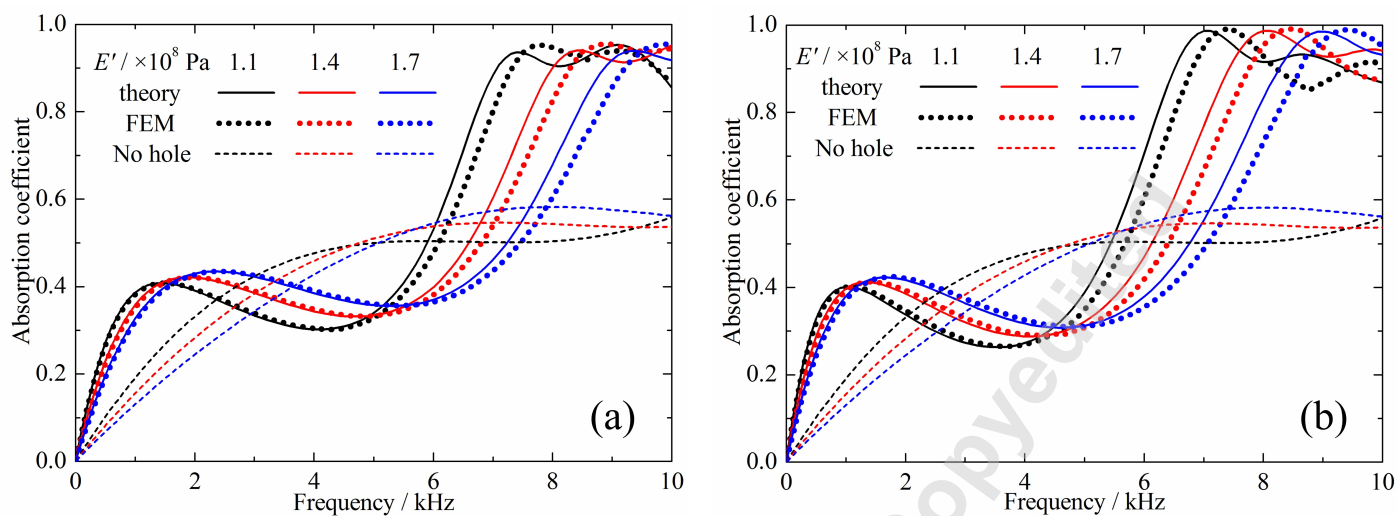


Fig. 5

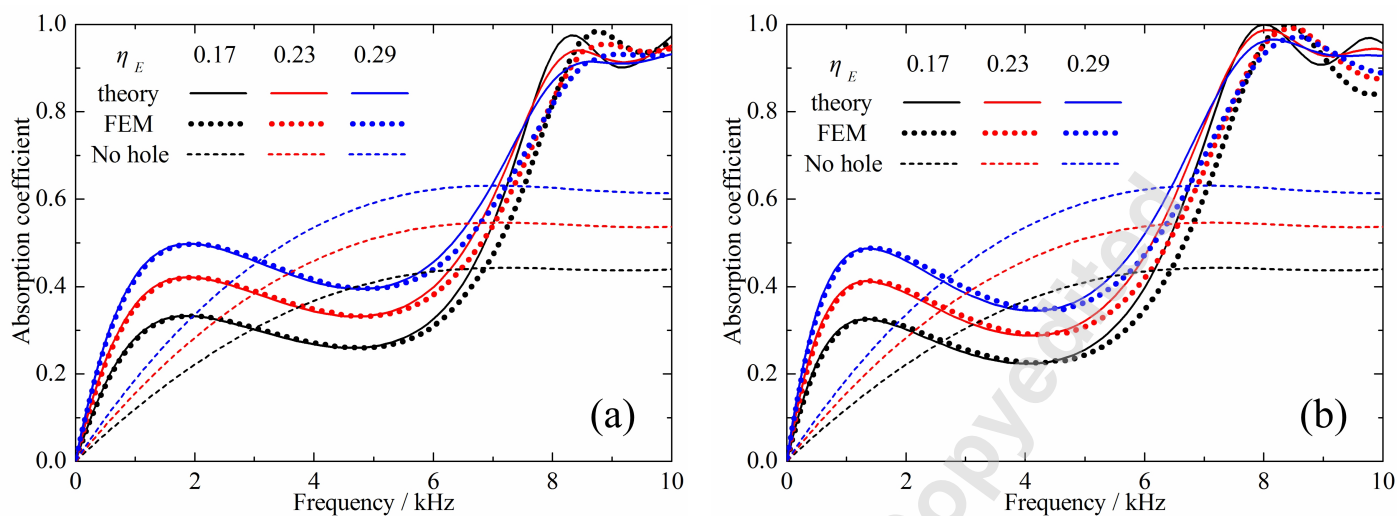


Fig. 6

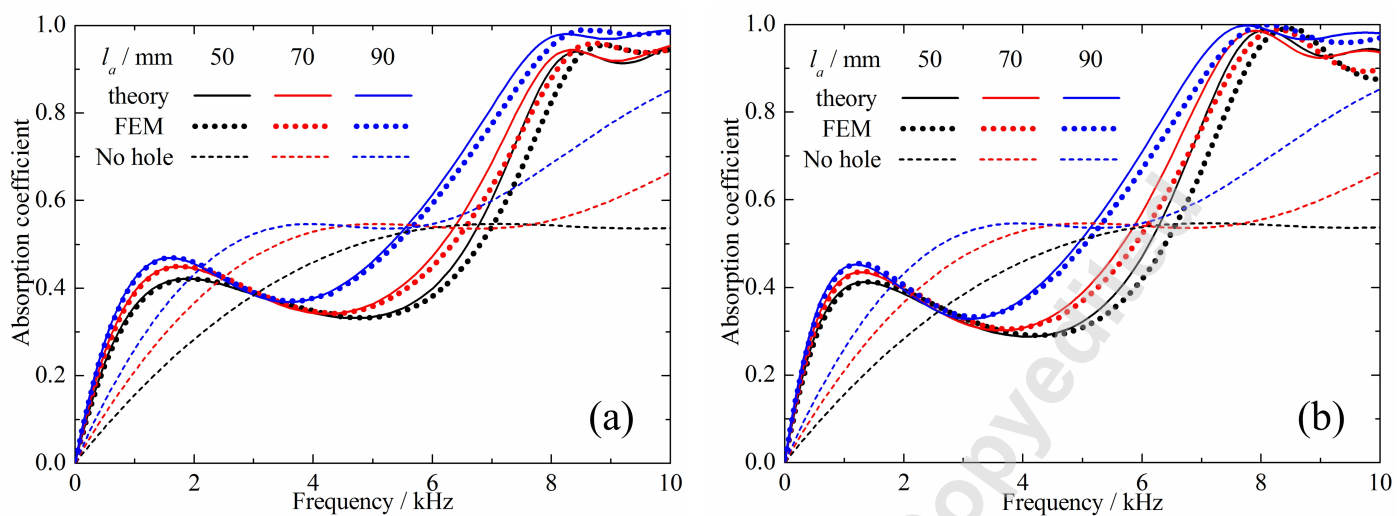


Fig. 7

Accepted Manuscript Not Copyable

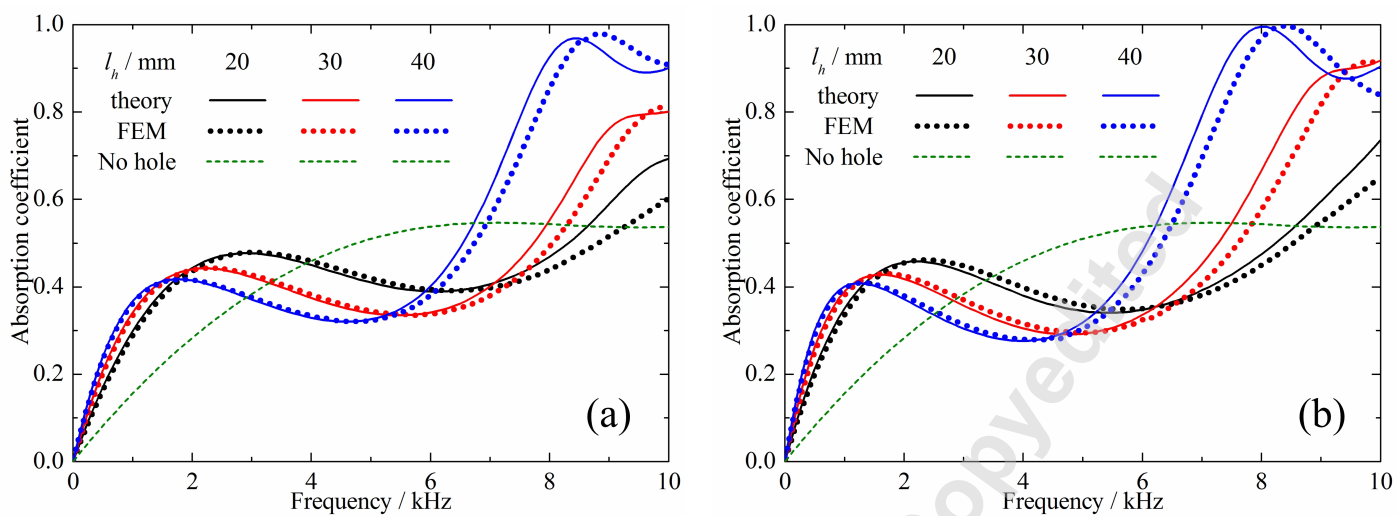


Fig. 8

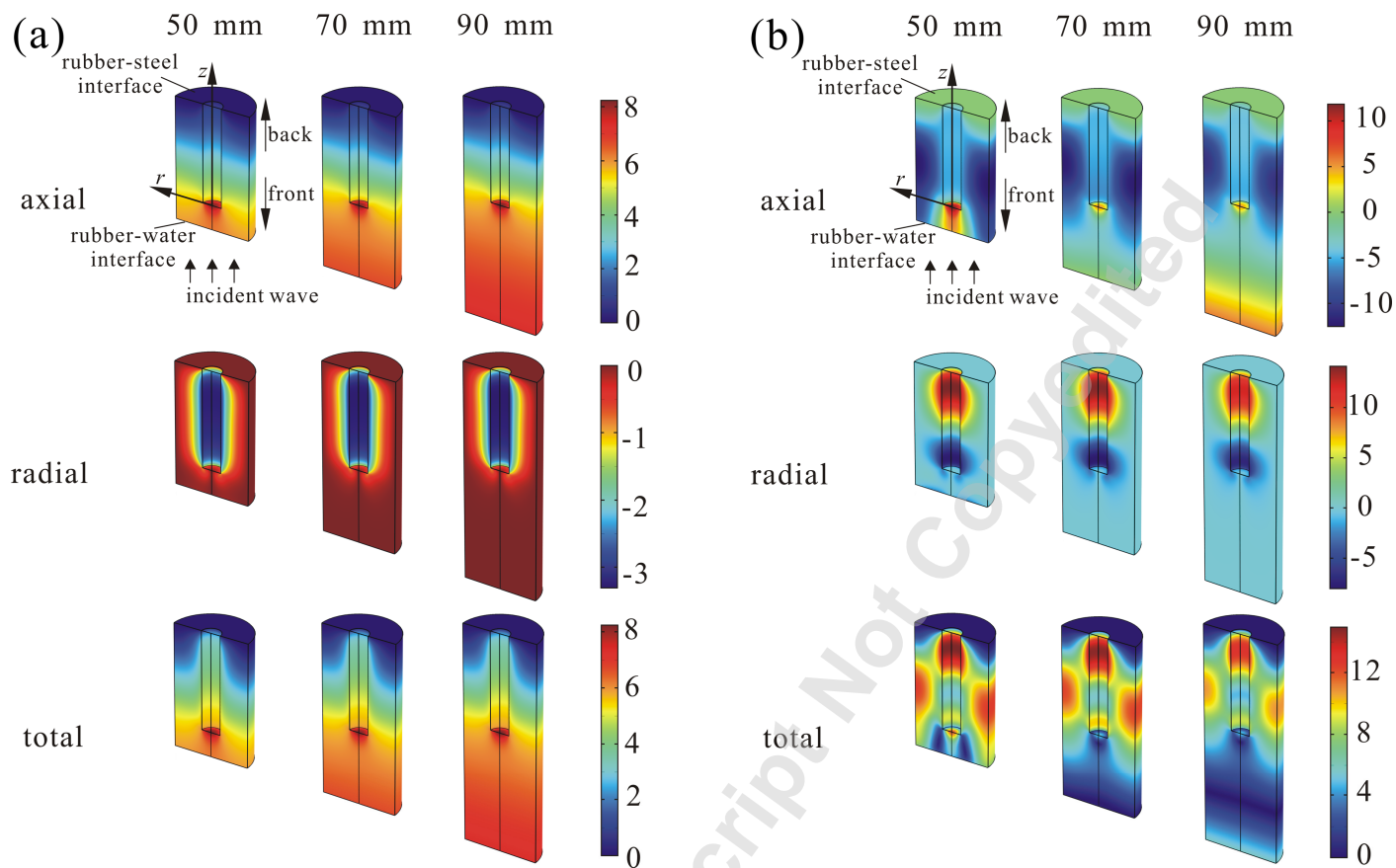


Fig. 9

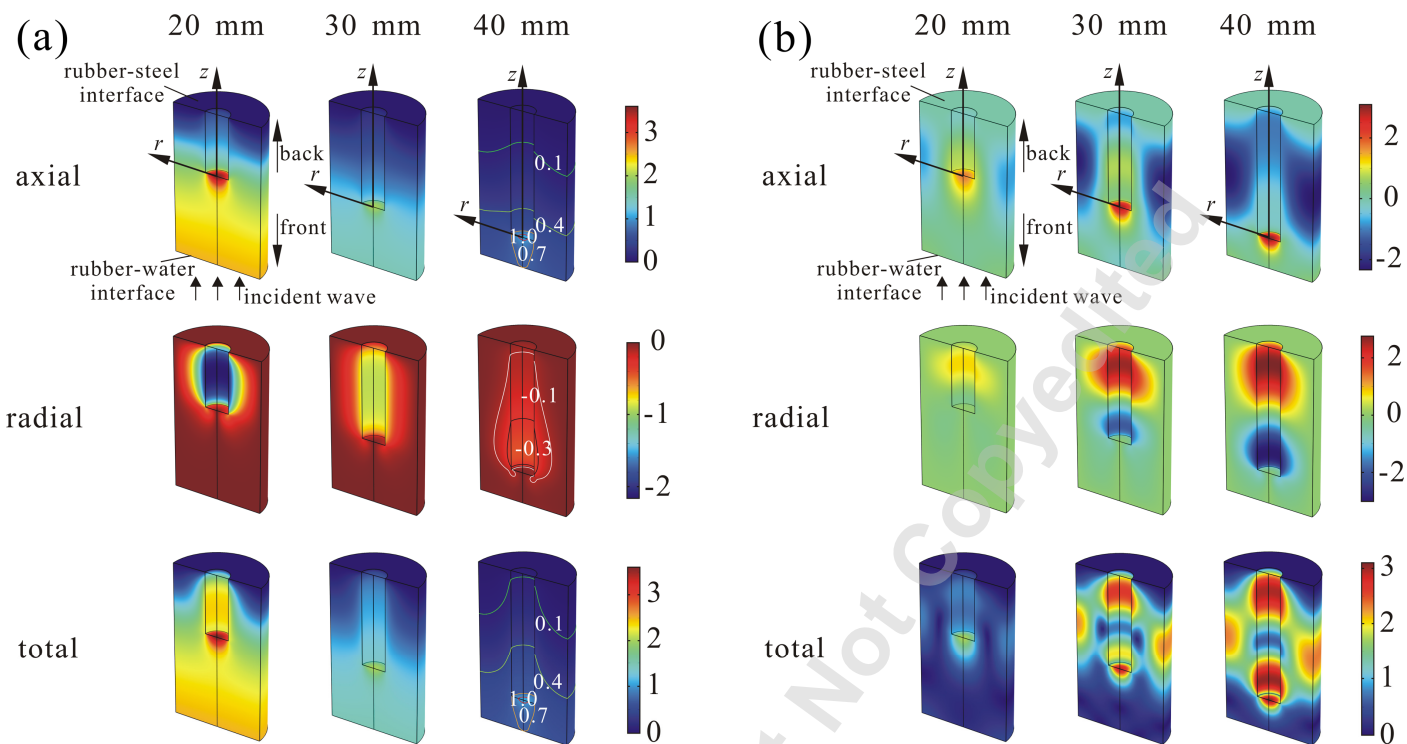


Fig. 10

Table 1

| Parameter | Symbol | Unit | Values | | |
|------------------------------------------|---------------------|---------------------------------|---------|---------|---------|
| | | | value 1 | value 2 | value 3 |
| Density of rubber | ρ | $\text{kg} \cdot \text{m}^{-3}$ | 900 | 1100* | 1300 |
| Real part of Young's modulus of rubber | E' | 10^8 Pa | 1.1 | 1.4* | 1.7 |
| Loss factor of Young's modulus of rubber | η_E | 1 | 0.17 | 0.23* | 0.29 |
| Thickness of anechoic layer | l_a | mm | 50* | 70 | 90 |
| Height of hole | l_h | mm | 20 | 30 | 40* |
| Poisson ratio of rubber | ν | 1 | | 0.49 | |
| Density of air | ρ_{air} | $\text{kg} \cdot \text{m}^{-3}$ | | 1.21 | |
| Density of water | ρ_w | $\text{kg} \cdot \text{m}^{-3}$ | | 998 | |
| Sound speed of water | c_w | $\text{m} \cdot \text{s}^{-1}$ | | 1483 | |

Accepted Manuscript Not Copyedited